

## **Aerodynamic design and evaluation of a ducted fan lift system for vertical takeoff and landing flying cars**

Jiang, Hanjie; Zhou, Ye; Ho, Hann Woei

**DOI**

[10.1177/09576509221106395](https://doi.org/10.1177/09576509221106395)

**Publication date**

2022

**Document Version**

Final published version

**Published in**

Proceedings of the Institution of Mechanical Engineers, Part A: Journal of Power and Energy

**Citation (APA)**

Jiang, H., Zhou, Y., & Ho, H. W. (2022). Aerodynamic design and evaluation of a ducted fan lift system for vertical takeoff and landing flying cars. *Proceedings of the Institution of Mechanical Engineers, Part A: Journal of Power and Energy*, 237(1), 115-125. <https://doi.org/10.1177/09576509221106395>

**Important note**

To cite this publication, please use the final published version (if applicable).  
Please check the document version above.

**Copyright**

Other than for strictly personal use, it is not permitted to download, forward or distribute the text or part of it, without the consent of the author(s) and/or copyright holder(s), unless the work is under an open content license such as Creative Commons.

**Takedown policy**

Please contact us and provide details if you believe this document breaches copyrights.  
We will remove access to the work immediately and investigate your claim.

## **Aerodynamic design and evaluation of a ducted fan lift system for vertical takeoff and landing flying cars**

Jiang, Hanjie; Zhou, Ye; Ho, Hann Woei

**DOI**

[10.1177/09576509221106395](https://doi.org/10.1177/09576509221106395)

**Publication date**

2022

**Document Version**

Final published version

**Published in**

Proceedings of the Institution of Mechanical Engineers, Part A: Journal of Power and Energy

**Citation (APA)**

Jiang, H., Zhou, Y., & Ho, H. W. (Accepted/In press). Aerodynamic design and evaluation of a ducted fan lift system for vertical takeoff and landing flying cars. *Proceedings of the Institution of Mechanical Engineers, Part A: Journal of Power and Energy*. <https://doi.org/10.1177/09576509221106395>

**Important note**

To cite this publication, please use the final published version (if applicable).  
Please check the document version above.

**Copyright**



Other than for strictly personal use, it is not permitted to download, forward or distribute the text or part of it, without the consent of the author(s) and/or copyright holder(s), unless the work is under an open content license such as Creative Commons.

**Takedown policy**

Please contact us and provide details if you believe this document breaches copyrights.  
We will remove access to the work immediately and investigate your claim.

# Aerodynamic design and evaluation of a ducted fan lift system for vertical takeoff and landing flying cars

Proc IMechE Part A:  
J Power and Energy  
2022, Vol. 0(0) 1–11  
© IMechE 2022  
Article reuse guidelines:  
[sagepub.com/journals-permissions](https://sagepub.com/journals-permissions)  
DOI: 10.1177/09576509221106395  
[journals.sagepub.com/home/pia](https://journals.sagepub.com/home/pia)  
SAGE

Hanjie Jiang<sup>1</sup> , Ye Zhou<sup>1,2</sup>  and Hann Woei Ho<sup>1,2</sup>

## Abstract

Urban air mobility is a relatively new concept that has been proposed in recent years as a means of transporting passengers and goods in urban areas. It encompasses a diverse range of Vertical TakeOff and Landing (VTOL) vehicles that function more like passenger-carrying drones for on-demand transportation. Among them, the car-like VTOL is advantageous due to its compact configuration, safe rotors, high user affinity, and technological fashion. These characteristics are frequently derived from the flying car's Ducted Fan Lift System (DFLS). This study aims to develop a method for the rapid design and the evaluation of the aerodynamic performance of the DFLS, to support the preliminary scheme demonstration of the ducted fan flying car. The proposed method uses blade element theory to design the unducted fan and applies momentum theory to calculate the aerodynamic thrust of the DFLS. The DFLS of a 1:3 scale verifier for a flying car scheme was designed and evaluated using the proposed method and a numerical method, respectively. To validate the proposed method, a prototype of the scale DFLS was manufactured and tested, and the result was compared with those of the proposed theoretical method and the numerical method. This study demonstrates that while both the theoretical and numerical methods are capable of designing an unducted fan accurately, the theoretical method is simpler and faster. Compared to the DFLS test results, the theoretical method's average difference is approximately 1.9%. When evaluating the DFLS, the accuracy of the numerical calculation is reduced, and the difference is greater than 30% at low power. The theoretical method presented in this paper can be used to improve the aerodynamic design and evaluation efficiency of the DFLS and to aid in the configuration evaluation of VTOLs equipped with ducted fans.

## Keywords

Ducted fan design, urban air mobility, vertical takeoff and landing, numerical calculation, flying car

Date received: 4 January 2022; accepted: 13 May 2022

## Introduction

In some movies and novels, flying cars appear, and they have long been an intuitive concept for urban aircraft. Many aircraft for urban flight have been built over the last 50 years, and some are still being developed.<sup>1</sup> The developed technologies have significantly increased the possibilities of Urban Air Mobility (UAM), which utilize passenger drones to transport people on-demand in urban environments, similar to how flying cars are imagined.<sup>2</sup> Different types of Vertical TakeOff and Landing (VTOL) vehicles are being developed based on the UAM concept, including multi-rotors, tilt-rotors, composite lift, and helicopters.<sup>3</sup> Flying cars frequently employ the multiple Ducted Fan Lift System (DFLS) installed inside the fuselage to ensure a feasible technical solution. As a result, a VTOL aircraft resembling a car has obvious advantages in terms of customer affinity, compact layout, and rotor safety.

The ducted fan has several advantages as a lift propulsion unit: high propulsion efficiency, high static thrust, good noise reduction, safety (in comparison to open propellers), and

controllable slip-stream diameter, all of which make the ducted fan viable for VTOL aircraft.<sup>4,5</sup> For VTOL aircraft, the design of the lift system is critical to ensuring the aircraft's reasonable configuration, flight safety, and flight performance. For ducted fan VTOLs, the dependency between the design parameters of the DFLS and of the aircraft is illustrated in [Table 1](#). Note that the aerodynamic force of the DFLS determines the aircraft's Center of Gravity (CG). This is because the lifting system must account for the CG to meet the longitudinal stability requirements of fixed-wing flight as well as the longitudinal balance requirements of VTOL. If the lifting system and the aircraft's CG are misaligned, the lifting

<sup>1</sup>School of Aerospace Engineering, Engineering Campus, Universiti Sains Malaysia, Nibong Tebal, Malaysia

<sup>2</sup>Faculty of Aerospace Engineering, Delft University of Technology, Delft, The Netherlands

### Corresponding author:

Ye Zhou, School of Aerospace Engineering, Engineering Campus, Universiti Sains Malaysia, Nibong Tebal, Pulau Pinang 14300, Malaysia.  
Email: [zhouye@usm.my](mailto:zhouye@usm.my)

system's thrust performance will be severely limited. In addition, the design parameters of the rotational speed of the DFSL will affect the design of the power and energy system. Specifically, if the DFSL is driven by a fuel engine, the required rotational speed will determine whether a transmission is required and also the parameters of the transmission. If the DFSL is driven directly by a motor, the KV rating (the ratio of the motor's rotational speed to the supply voltage) determines the supply voltage of the motor. That means that KV rating directly determines the current, the capacity and the weight of the power battery at a certain motor output power. As a result, it is critical to enhance the efficiency and accuracy of the design of VTOL aircraft lift systems.

Although the ducted fan has tremendous potential, it is difficult to analyze its aerodynamic properties due to the complexity of its geometry. Factors such as duct-lip curvature, duct length, and duct diffuser angle must all be considered when designing an efficient ducted fan.<sup>6,7</sup> Models of ducted fans are constructed in some literature<sup>5,8,9</sup> using momentum theory. However, the majority of these models are used to describe the lifting principle and the composition of the lifting force; they are rarely used to directly design or evaluate the lifting system. As an alternative, numerical analysis is frequently used to design and evaluate the ducted fan's aerodynamic performance.<sup>4,10,11</sup> One of the advantage of using the numerical analysis is that it is able to predict and evaluate the aerodynamic force interaction between the fan and the duct. Additionally, it could reflect the ducted fan's design details and allow for design optimization. However, the numerical

method takes a long time to compute, and the calculation accuracy depends on the chosen numerical model. After tuning the model parameters, complex calculations must be repeated, which does not meet the requirement for rapid iteration in the preliminary design and evaluation of a ducted fan VTOL. As a result, a new design methodology for the ducted fan used in VTOL is required.

This paper proposed a novel type of VTOL flying car that is propelled by ducted fans and tilting rotors. The flying car is a four-seat urban area commuter aircraft with a take-off weight of about 2700 kg and a wingspan about 6.5 m. As illustrated in [Figure 1](#), the flying car's rear frame is equipped with four sets of ducted fan systems. The first phase of the project will involve the development of a 1:3 scale flying car demonstrator for the purpose of validating the aerodynamic configuration and flight control system. This article will focus on the aerodynamic design and evaluation of the DFSL, as illustrated in [Figure 2](#). Certain fundamental requirements for achieving these characteristics dictate the aerodynamic performance of the sub-scale ducted fan, as illustrated in [Table 2](#).

This paper is primarily concerned with rapid designing and evaluation the aerodynamic performance of the DFSL for the VTOL preliminary design. The flow chart in [Figure 3](#) illustrates the aerodynamic design method for the DFSL proposed in this paper. As illustrated in the figure, the first step is to calculate the static thrust of the unducted fan in relation to the static thrust demand of the ducted fan. The momentum theory is used to define the ducted fan system's overall thrust characteristics and the composition of its

**Table 1.** Dependency between the design parameters of the VTOL and its DFSL.

Design parameters of the DFSL	Design parameters of the VTOL
Geometry	Contour Configuration
Aerodynamic forces	Flight performance CG design Configuration
Power absorbed	Weight and size of the engine/motor Weight and volume of the fuel/battery
Rotational speed	Weight and size of transmission Weight and volume of the battery Noise constraints

VTOL: Vertical TakeOff and Landing; DFSL: Ducted Fan Lift System.



**Figure 1.** The flying car Vertical TakeOff and Landing concept.

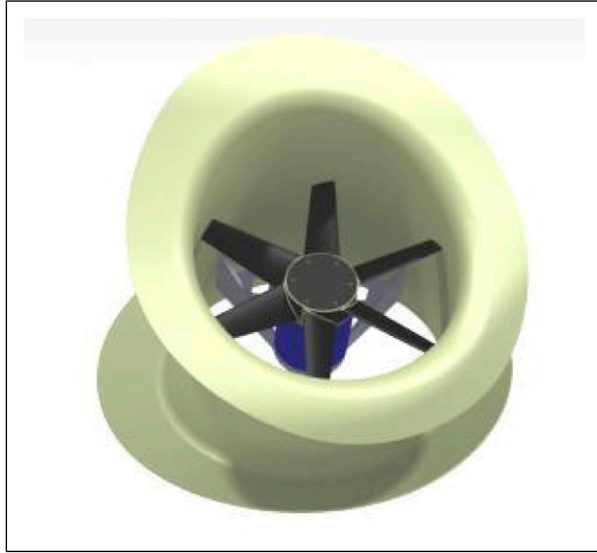


**Figure 2.** The model of the ducted fan lift system.

**Table 2.** Principal design characteristics.

Characteristic	Value
Diameter of duct	330 mm
Duct length (Central axis)	330 mm
Diameter of fan	326 mm
Maximum static thrust	300 N
Maximum power	13500 W
Density of air	1.225 kg/m <sup>3</sup>
Viscous coefficient	0.017894 g/lms
Ambient pressure	101.3 kPa

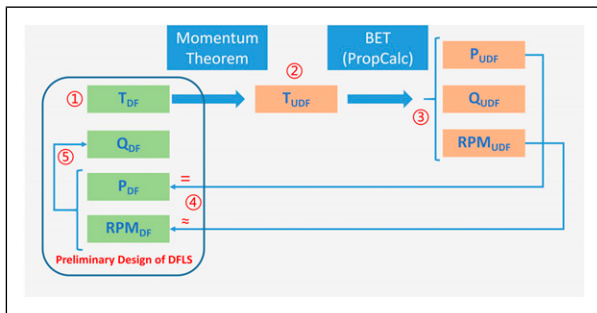


**Figure 3.** Flow chart of the theoretical aerodynamic design method of DFLS in hover (The subscript UDF stands for an unducted fan, and the subscript DF stands for a ducted fan). DFLS: Ducted Fan Lift System.

forces. The unducted fan is then designed using the Blade Element Theory (BET). Simultaneously, the unducted fan's power and rotational speed performances can be used to predict the DFLS's performance. Additionally, the torque of the ducted fan system can be estimated using this method. *Theoretical design of the DFLS* of this paper discusses the theoretical design method. In *Numerical design of the DFLS*, the aerodynamic performance of the ducted fan is also evaluated numerically using CFD. *Static Bench Test* includes a force test on the DFLS prototype to verify the theoretical method's feasibility. *Results analysis* of this

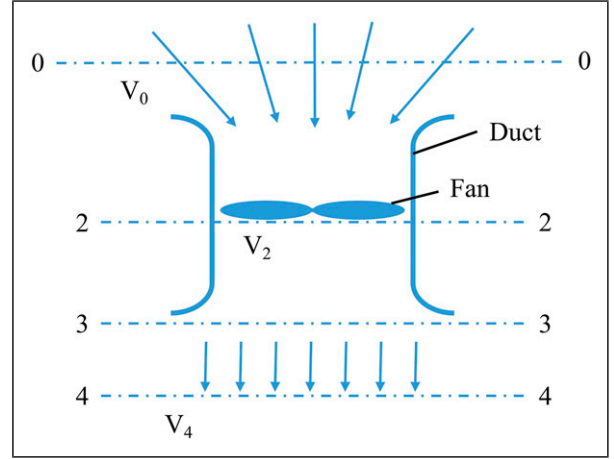


**Figure 4.** The model of the ducted fan lift system.

paper analyzes and compares the design results for the DFLS demonstrator using the three design methods.

### Theoretical design of the DFLS

To better illustrate the DFLS, this section first introduces a momentum model to present its components and their relationships. Following that, the BET and unducted fan designs are introduced, corresponding to the third design step in Figure 3. Finally, using momentum theory, the relationship between the thrust performance of an unducted fan and a ducted fan is established, corresponding to the second and fourth steps in Figure 3.

#### Ducted fan lift system model in hover based on the momentum theory

As shown in Figure 4, with the incoming flow velocity  $V_0 = 0$ , the total thrust of the lift fan system can be written as<sup>8</sup>

$$T = T_{FID} + T_D = \rho S_2 V_2 V_4 = \rho \sigma S_2 V_4^2 \quad (1)$$

$$V_2 = \sigma V_4 \quad (2)$$

where  $\rho$  is the air density,  $S_2$  is the area of the fan disc,  $V_2$  is the velocity just under the fan, and  $V_4$  is the far wake velocity. The subscript  $FID$  stands for a fan in the duct, and the subscript  $D$  stands for a isolate duct. The duct diffusion ratio  $\sigma$  is often chosen as  $\sigma \in [0.5, 1]$  for a ducted lift fan and  $\sigma = 0.5$  for an unducted fan.

The thrust of the fan in the duct can be written as

$$T_{FID} = S_2(\Delta p) = \frac{1}{2} \rho S_2 V_4^2 \quad (3)$$

$$\frac{T_{FID}}{T} = \frac{1}{2\sigma} \quad (4)$$

and the output power of the DFLS is

$$P\eta = T_{FID}V_2 = \sigma T_{FID}V_4 = \frac{T^{\frac{3}{2}}}{\sqrt{4\sigma\rho S_2}} \quad (5)$$

where  $\eta$  is the fan efficiency.

The momentum theorem model is capable of clearly expressing the DFLS's static aerodynamic thrust, power, and

thrust composition. It is, however, difficult to apply directly to the design of a ducted fan. As a result, it is necessary to use propeller theory to benchmark the performance of an unducted fan. The aerodynamic effect of the duct on the fan is then clarified to complete the DFLS's preliminary design.

### Fan design based on BET

According to the BET, propellers are composed of infinitesimal elements in the shape of airfoils along each blade's radius,<sup>9</sup> as illustrated in Figure 5. The resulting velocity for each element can be decomposed into rotational and translational components and the resulting aerodynamic force into drag and lift. When decomposed in the plane of rotation, it produces thrust and the torque-producing force. Nonetheless, because these aerodynamic reactions involve a blade element, they must be treated as infinitesimal, as illustrated in Figure 5.

The expression for the lift in the elementary profile can be represented as

$$dL = \frac{1}{2} \rho V_r^2 C_L b \cdot dr \quad (6)$$

where  $L$  is the lift, and the subscript  $r$  stands for rotation. By the geometry in Figure 5, it is given that

$$dL = dR \cdot \cos \gamma \quad (7)$$

$$dR = \frac{1}{2} \frac{\rho V_{trans}^2 C_L b \cdot dr}{\sin^2 \phi \cos \gamma} \quad (8)$$

where  $R$  is the resultant force and the subscript  $trans$  stands for translation. Thus, the infinitesimal thrust produced by the considered element is given by

$$dT = dR \cdot \cos(\phi + \gamma) \quad (9)$$

$$dT = \frac{1}{2} \frac{\rho V_{trans}^2 C_L b \cdot dr}{\sin^2 \phi \cos \gamma} \cdot \cos(\phi + \gamma) \quad (10)$$

For simplification, the thrust coefficient,  $T_c$ , is introduced as follows

$$T_c = \frac{C_L b}{\sin^2 \phi \cos \gamma} \cdot \cos(\phi + \gamma) \quad (11)$$

The expression of the total thrust can be obtained by integrating equation (10) over the radius

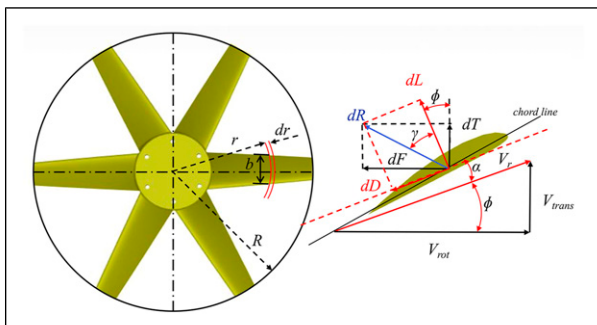


**Figure 5.** Infinitesimal airfoils along the blade radius on the left and different settings concerning each element on the right.

$$T_{UDF} = \frac{1}{2} \rho V_{trans}^2 B \int_0^R T_c \cdot dr \quad (12)$$

where  $B$  is the blade number corrective factor. The horizontal component  $dF$  of the total aerodynamic force causes the torque  $dQ$ , which can be written as

$$dQ = r \cdot dF \quad (13)$$

$$dF = dR \cdot \sin(\phi + \gamma) \quad (14)$$

Accordingly, the total torque can be written as

$$Q_{UDF} = \frac{1}{2} \rho V_{trans}^2 B \int_0^R Q_c \cdot dr \quad (15)$$

The rate of energy supplied by the motor matches its power

$$P_{UDF} = 2\pi n Q \quad (16)$$

It should be noted that equations (12), (15), and (16) estimate the properties of the unducted fan in a specific state solely based on the fan's geometry, fluid dynamics, and kinematics.

At the moment, several propeller design tools are available, most of which are based on BET. Rather than developing a new propeller design program, this study relied on PropCalc,<sup>12</sup> a classic propeller design software.

Table 3 contains the design parameters for the fan used in this study. PropCalc can be used to determine the thrust, absorbed power, and efficiency of an unducted fan at various rotational speeds. *Static Bench Test* will present the fan's performance evaluation results, which will be compared and analyzed alongside the numerical calculation and test results.

### Action of duct

Several studies have been published in the literature reporting the influence of a duct on the aerodynamic forces of the DFLS in hover state. GRAHAME<sup>13</sup> investigated to determine the force contribution of V/STOL lift-fan inlets based on momentum theory. In GRAHAME's model, the proportion of  $T_{duct}$  in hovering is constant 0.5, i.e.  $\sigma = 1$  in equation (4). Additionally, Platt<sup>14</sup> gives the static thrust ratio between the ducted fan and the unducted fan with the same absorbed power using the simple momentum theorem.

**Table 3.** Fan design parameters.

Airfoil	Diameter	Blades
CLARK-Y	326 mm	6
% Of radius	Chord (mm)	Blade angle (deg)
20	54	35
30	51	34
40	48	33
50	45	32
60	42	31
70	39	30
80	36	29
90	33	28
100	30	27

This ratio is a function of the fan disc area  $S_2$  and the duct outlet area  $S_4$ , verified by experimental tests.

Along with theoretical research, some numerical studies are used to analyze the effects of ducts. Jiang et al.<sup>4</sup> used Computational Fluid Dynamics (CFD) simulations to evaluate a novel annular-DFLS for VTOL aircraft. Sheng et al.<sup>15</sup> used a high-fidelity three-dimensional unsteady Reynolds-averaged Navier-Stokes (RANS) flow solver based on unstructured grid technology to investigate the aerodynamic performance of a fan-in-wing system. Xu et al.<sup>16</sup> investigated the complex flows surrounding ducted and isolated propellers in a ducted fan by solving unsteady Euler equations using unstructured dynamic overset grids.

It is difficult to extract general rules from the DFLS performance research and express them mathematically using the numerical calculation method. As a result, this paper used the findings from Platt's study to establish the primary design method for a DFLS. The momentum theorem used in the literature is also applicable to this study, with the following two assumptions: the flow is incompressible and frictionless, and the static pressure of the air exiting the duct has reached free-stream pressure. While the total pressure immediately behind the propeller is equal to the pressure at the duct's exit.

The main theoretical result of Platt's study can be presented by the equation below,<sup>14</sup>

$$\frac{T_{DF}}{T_{UDF}} = 1.26 \left( \frac{S_3}{S_2} \right)^{\frac{1}{3}} \quad (17)$$

Equation (17) premise is that the fan in the duct and the isolated fan have equal absorption power, that is  $P_{DF} = P_{UDF}$ .

## Numerical design of the DFLS

In this paper, numerical calculations are also used to evaluate the customized ducted fan in order to demonstrate the theoretical method's practicality through comparison. The numerical results can be used to determine the pressure and airflow characteristics of the components, assisting in the optimization of a DFLS. Between the preliminary and detailed design phases, these detailed results are required.

## Computational method

The computational method used for designing the DFLS is based on the high-fidelity three-dimensional quasi-steady RANS CFD method. This paper employs a finite volume, fully unstructured grid technology to model and simulate both internal and external viscous flows, including dynamic relative motions, in the ducted fan or fan-in-wing configurations. Calculations were performed using the ANSYS CFX. The turbulence model utilized is  $k - \omega$  SST (Shear Stress Transport) model, with high simulation precision for adverse pressure gradient flow simulation. The second-order high-resolution method is adopted for spatial dispersion, and both the convection and the turbulence terms adopt the second-order accurate numerical discretization scheme.

## Computational grid

The sliding grid is used in this paper to consider the overall consumption of computing resources and calculation methods.<sup>17</sup> The off-body grid system used in the study extend 50 fan radii from the origin in the up-down direction and 30 fan radii in the radial direction. Only the fan is the moving part in the CFD calculation of an unducted or ducted fan, and only the area around the fan needs to be separated. For sliding meshes, the rotating region should be configured so that the local motion speed does not penetrate the mesh. For simplicity, the rotational region is defined as the region of the cylinder enclosing the fan, as illustrated in Figure 6. The boundary condition of the far-field grid surface is set as the pressure far field, and the boundary condition of the duct and fan surfaces is set as the no-slip surface boundary. The interface boundary condition is adopted between the far-field grid and the near-field grid. Table 4 lists the number of numerical calculation grids. The object surface y plus is about 20–30, and the grid around the object surface is refined. The grid near the wake of the leading and trailing edge of each blade is also refined, and the size is 0.002–0.005 times the chord length. Figure 7 illustrates the computational grid for the ducted fan.

## Numerical simulation results

The hovering performance of both ducted and unducted fans is evaluated numerically in this paper. The pressure contour on the mid-plane of the fans at the same rotational speed is shown in Figure 8. The results show that the isolated fan has a stronger vortex behind the blade tip compared to the ducted fan, which indicate that that the duct's inner shell improves the flow around the fan blade tip region. Additionally, the flow around the duct's inlet leading edge creates a large negative pressure area, which results in significant additional duct thrust. After adding a duct to the outer fan ring, the pressure distribution in the

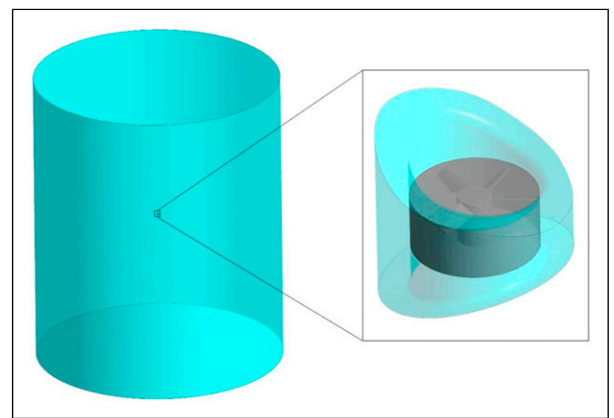


**Figure 6.** Grid region division (partial enlargement on the right).

**Table 4.** Number of grid cells.

Parameters	UDF	DF	Far-field region
Element number	15.75 M	17.32 M	2.37 M

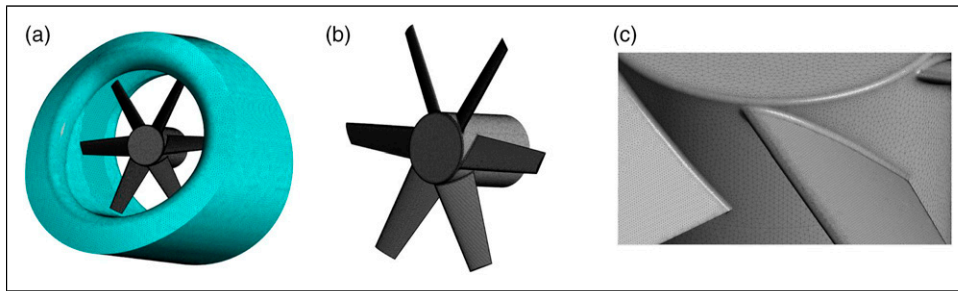


**Figure 7.** Ducted fan computational grid.

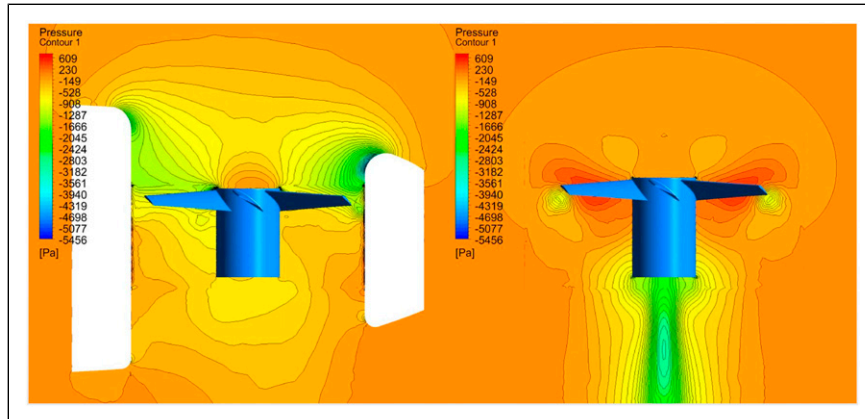


**Figure 8.** Pressure contour on the mid-plane of the ducted fan on the left and of the unducted fan on the right.

fan disc area changed significantly. The primary reason for this is that the airflow accelerates rapidly at the duct inlet before passing through the fan, resulting in an increase in the inflow velocity directly ahead of the fan. The pressure contour on the upstream surface of the fans is depicted in Figure 9. The fan's thrust in the duct is less than that of the isolated fan at the same rotational speed.

Figure 10 illustrates the speed contours of unducted and ducted fans operating at the same rotational speed. The results show that the ducted fan's slipstream velocity is less than that of the isolated fan at the same rotational speed indicating that the duct modifies the fan's slipstream state and aerodynamic efficiency. As illustrated in Figure 11, there are obvious differences in the streamline morphology of ducted and unducted fans. The fan pumps the airflow, which converges on the fan from above and around via the duct lip. At the lip, the airflow along the duct's surface accelerates, causing the airflow directly above the fan to accelerate as well, transforming the original centripetal convergent airflow into a columnar downflow.

### Static bench test

To validate the aerodynamic design results of DFSL, a 326 mm diameter fan and a 330 mm inner diameter duct shell were manufactured, along with the corresponding brushless motor, electric speed controller, and electric battery. Bench testing was conducted using the customized brushless motor, electric speed controller, and electric battery. The test bench is a piece of laboratory equipment that is used to determine the static-dynamic characteristics of various propulsion units using a box balance and a VXI. This

section primarily introduces the test method and equipment; *Results analysis* discusses the test results.

### Ducted fan model and its installation

The duct shell is constructed entirely of carbon fiber composite material to ensure the required shape accuracy and stiffness. Additionally, the fan is constructed of carbon fiber composite material. The fan is formed in one piece using a single mold to ensure that each blade is installed accurately and meets the specified strength requirements. As a high-speed rotating part, the fan needs static and dynamic balance adjustment after machining, as shown in Figure 12. The fan blades use the Clark-Y airfoil with a twist angle of 8 deg from root to tip. The inlet lip and the outer edge of the duct fit the contour of the flying car.

As illustrated in Figure 13, the ducted fan system is installed on the test bench for static performance testing. A 15 KW brushless external-rotor motor mounted in the duct drives and supports the fan. Metal support connects the motor and the duct shell and secures them together on a metal platform. The metal platform is mounted on top of a frame-type force balance, which is used to measure thrust and torque throughout the DFSL. When testing the fan separately, the duct shell can be removed. The duct shell can be removed when the fan is tested separately.

### Measuring equipment and data acquisition

A six-component box balance was used in the test to measure the performance of the DFSL, and its specific



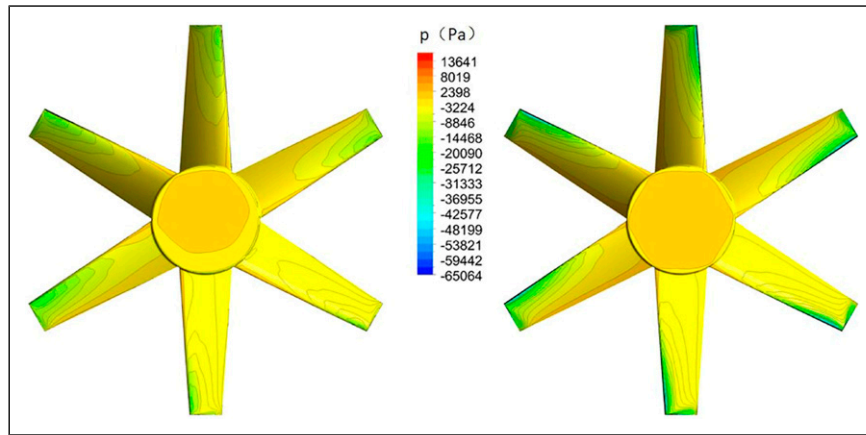


Figure 9. Pressure contour on the upstream surface of the ducted fan on the left and of the unducted fan on the right.

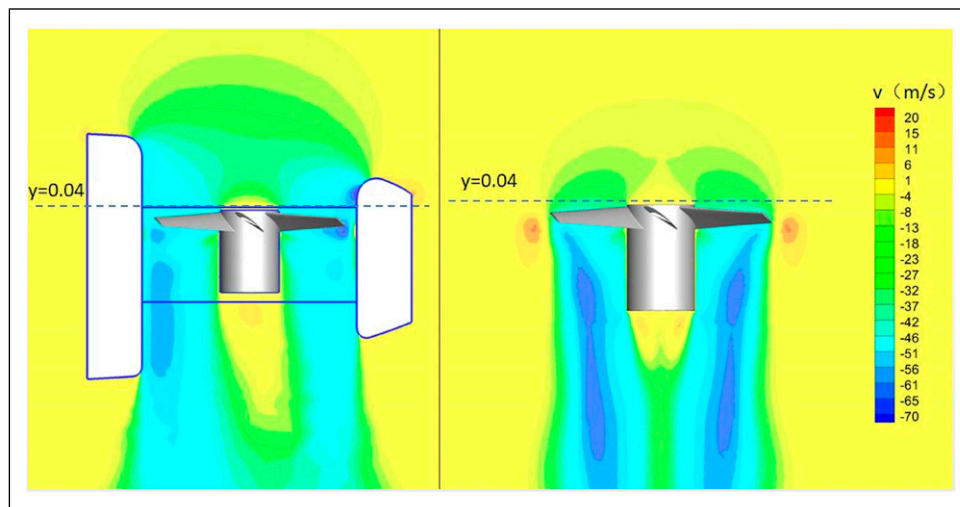


Figure 10. Speed contour on the mid-plane of the ducted fan on the left and of the unducted fan on the right.

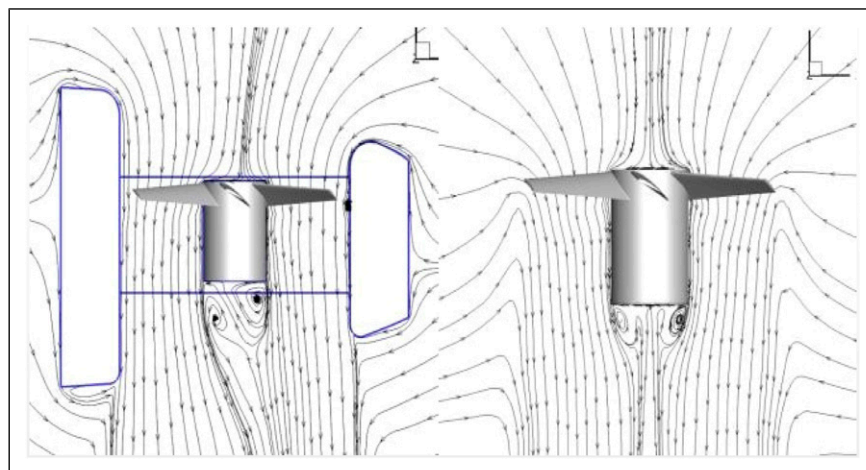


Figure 11. Streamlines on the mid-plane of the ducted fan on the left and of the unducted fan on the right.

technical parameters are shown in Table 5. A 32 channels VXI system was used for test data acquisition, and its acquisition speed is no less than 100 kHz/channel. The test voltage and current were measured and recorded to obtain the input power of the drive motor. The voltmeter is an MF35 multimeter. The ammeter is a VIVTOR6056 E

ammeter. A Hall type rotational speed measuring unit is installed on the motor, whose error is lower than 0.5%. The absorbed power of the fan can be calculated by multiplying the rotational angular rate of the motor and the corresponding fan torque measured by the VXI system, which was calibrated before each test.

## Results analysis

This section compares and analyzes the static-dynamic performance predicted by the theoretical and numerical methods with the test results. These analyses include the unducted fan and ducted fan design results. Finally, the authors discussed how to determine the rotational speed when designing the DFLS using the theoretical method. The theoretical method, numerical calculation method, and test are compared for performance under standard atmospheric conditions. As a result, the test data used in this paper has been corrected for comparison purposes.

### Results and comparisons of the unducted fan performance

The basic data of hovering performance for the unducted fan under standard atmospheric conditions are shown in

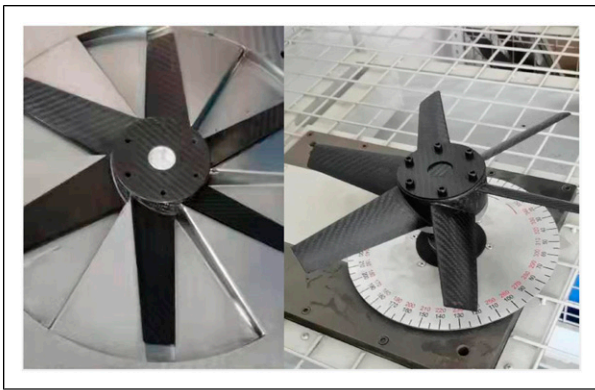


**Figure 12.** Carbon fiber fan and its installation on the balance test platform.

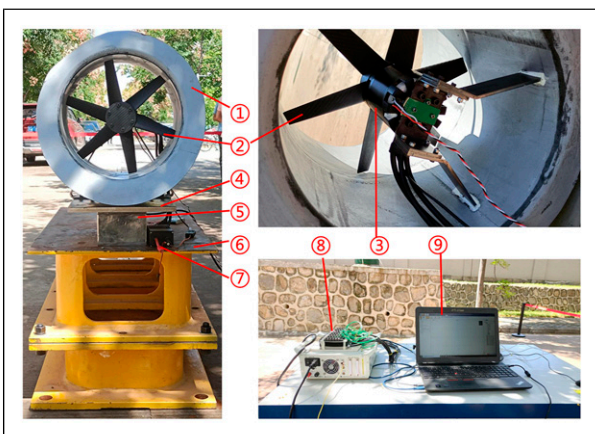


**Figure 13.** Ducted fan system installed on the test bench (1: duct shell, 2: fan, 3: motor, 4: metal platform, 5: balance, 6: test bench base, 7: electronic speed controller, 8: data acquisition system, 9: test data monitor).

**Table 5.** Technical parameters of the box balance.

Translational and rotational directions	Y	X	Z	$M_Y$	$M_X$	$M_Z$
Design load (N, Nm)	$\pm 5000$	$\pm 1200$	$\pm 500$	$\pm 300$	$\pm 300$	$\pm 800$
Calibration load (N, Nm)	$\pm 4511.1$	$\pm 1098.3$	$\pm 451.1$	$\pm 274.6$	$\pm 274.6$	$\pm 725.7$
Composite loading repeatability	0.017	0.060	0.072	0.059	0.004	0.005
Combined loading error	0.03	0.11	0.16	0.06	0.03	0.03

Figures 14–16. The thrust results for the fan are shown plotted against both their respective rotational speed and absorbed power, and the torque results are shown plotted against the respective rotational speed.

As illustrated in Figure 14, the theoretical and numerical results for thrust versus rotational speed agree well with the test results. The numerical calculation results in more precise performance, and the thrust at the same speed is slightly less than the test results, with an average difference of 5.6% and a maximum difference of 10.8%. The theoretical calculation is based on some simplified assumptions, and the calculated thrust values are greater than the measured values by an average of 8.6% and a maximum of 12.7%. The accuracy of the adopted numerical method is high which proves that the CFD method adopted in this paper is applicable to this study.

Figure 15 plots the thrust performance against the unducted fan's absorbed power, which can be used to determine the aerodynamic force efficiency. Blade Element Theory's power thrust curves are in good agreement with the test results and have a higher degree of precision. The thrust is marginally higher than the test results at the same power, with an average difference of 5.4% and a maximum difference of 6.7%. When the rotational speed is low, the efficiency is lower than the test results; however, when the rotational speed is high, the efficiency is greater than the test results. The maximum difference in numerical calculation for efficiency is approximately 28.5%.

As a result, Figure 16 depicts the torques generated by the unducted fan as a function of rotational speed, which corresponds to the results in Figures 14 and 15. The torque value obtained through theoretical calculation is closer to the experimental values, particularly at high rotational speeds exceeding 9000 r/min.

From the results given in Figures 14–16, the comparison can be concluded as follows: 1. The numerical calculation method adopted in this paper is verified by calculating the performance of the unducted fan, which can accurately evaluate the fan's performance. 2. Compared with the test results, the fan's performance calculated by BET is also accurate, and the torque prediction by BET is more accurate than that by numerical calculation.

### Results and comparisons of the ducted fan performance

After determining the isolated fan's aerodynamic performance using the theoretical method, the DFLS thrust data can be obtained almost synchronously. On the other hand, numerical calculations are much more time-consuming.

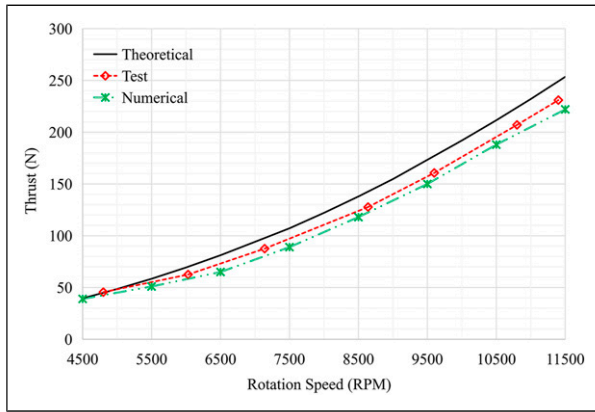


Figure 14. Unducted fan thrust against rotational speed.

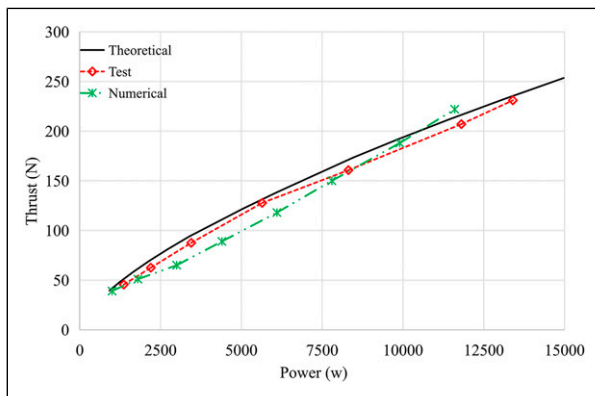


Figure 15. Unducted fan thrust against power.

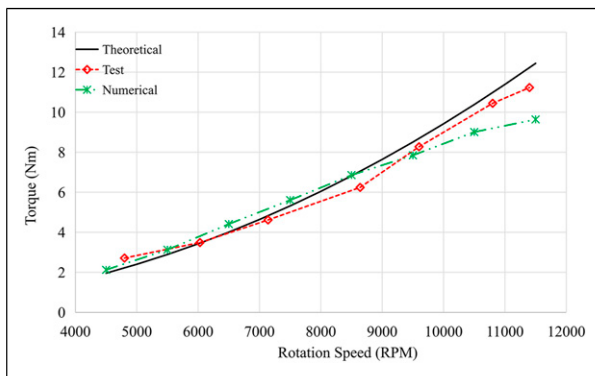


Figure 16. Unducted fan torque against rotational speed.

The reason is that all the steps, including model pre-processing, grid generation, calculation setup, numerical calculation, and the result post-processing, will need to be repeated to evaluate the fan with a shrouded duct. The final thrust power curves of the DFSL from the theoretical method, test, and numerical calculation are shown in Figure 17. When the test curve is compared to the theoretical results, it is determined that the theoretical results are reasonably accurate, with an average difference of 1.9% and a maximum difference of 5.8%. The precision of numerical calculation is lower; at low power, the difference is greater than 30%, but the accuracy improves with increasing power.

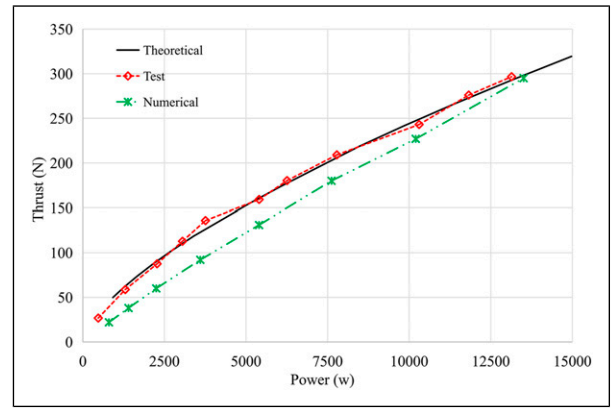


Figure 17. Ducted fan thrust against power.

### Rotational speed

The rotational speed is discussed in this section because it plays a critical role in designing a DFSL-driven unit. If the DFSL is powered by a motor, the required rotational speed performance of an electrical fan will determine the motor's KV rating and the power battery. On the other hand, if the DFSL is powered by an engine, the engine transmission will be selected in accordance with the required rotational speed. These are critical for the primary design of the flying car, particularly for determining the feasibility of the power system operating at the maximum output while hovering.

Although the speed performance of a ducted fan can be evaluated by using CFD analysis or the real-world test, these two methods currently cannot meet the requirement of the rapid iteration of the preliminary design. On the other hand, if the proportion of the thrust of an unducted fan with respect to the total thrust is known, the rotational speed can be predicted from the theoretical perspective. This proportion, however, will vary depending on different DFSL and their working conditions. In other words, it is hard to determine the rotational speed law of a DFSL using theoretical methods. Therefore, this paper proposes to find a simple approximation method to predict the maximum rotational speed of the DFSL in the hovering condition for the preliminary design.

Figure 18 plots the rotational speed of the fans against their power consumption. At low power values, the ducted fan's rotational speed is significantly faster than the unducted fan's, as illustrated in the figure. As power increases, the rotational speed differential decreases gradually. When the power is approximately 12.5 kW, both fans rotate at approximately 11,000 r/min. At high power, the rotational speed difference between the fan in the duct and the unducted fan is small. Xu's study<sup>16</sup> also obtained a similar result. The torque coefficient difference between the ducted fan and the isolated fan is negligible when the ducted fan is hovering at 8000 r/min.

For example, the aforementioned prototype is driven by a customized DC motor with a maximum output power of 15 KW, rated voltage of 96 V, and KV rating of 140. Assuming the difference between the actual and estimated speeds is 500 r/min, the KV rating deviation is around 5. And on the other way around, if the KV rating is fixed, the voltage deviation will be between 3 to 4 V.

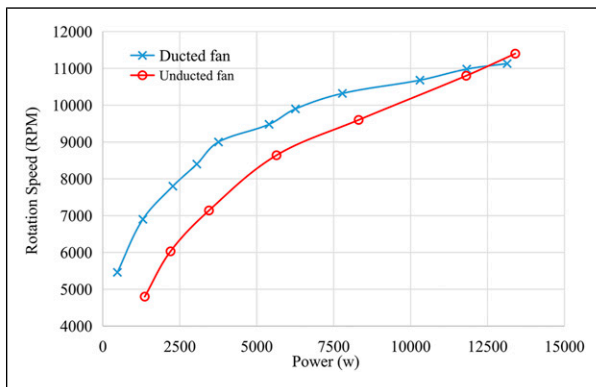


**Figure 18.** Ducted and unducted fan rotational speed against power in the static bench test.

When designing the motor, the margin, which is much larger than the above-mentioned deviation, need to be taken into account due to the decreased efficiency in use. In short, the initial rotational speed of the ducted fan in hover can be estimated using the rotational speed of the unducted fan with the same power, which can be used to customize the DFLS prototype.

More specifically, as shown in Table 2, the maximum thrust requirement of DFLS is 300 N, and the corresponding maximum thrust of the unducted fan calculated from equation (17) is about 236 N. The corresponding absorbed power of the unducted fan is 13,750 W by checking Figure 15, and equals the absorbed power of the DFLS with maximum thrust. Then the rotational speed of the unducted fan can be found in Figure 14, which is about 11,100 r/min. The corresponding KV rating of this rotational speed is about 117 when supplied at 96 V. Considering the difference between the motor idling speed and the rotational speed with load, about 20% margin was given in the design of the KV rating. The results in Figure 18 show that the estimation of the maximum rotational speed using the proposed method is in accordance with the real-world test.

## Conclusion

This paper establishes an aerodynamic performance design and evaluation method for the DFLS in a flying car project based on the BET and the momentum theory. The BET is used to design and evaluate the performance of the unducted fan, and the thrust performance of the DFLS is calculated using momentum theory. The ducted fan's hovering rotational speed was approximated using the isolated fan's result. Notably, the thrust characteristics of the ducted fan can be calculated using equation (17) from the data for the unducted fan. This results in an extremely efficient and intuitive theoretical design and evaluation for DFLS. Furthermore, the most striking result of the test validation is that this design and evaluation way is accurate. This study illustrated the development of a method for the rapid design and evaluation of the aerodynamic performance of the DFLS, which can efficiently support the preliminary scheme demonstration of a ducted fan flying car.

This method was specifically used to design and evaluate the DFLS of a 1:3 scale verifier. The isolated fan's aerodynamic performance is calculated using the traditional propeller design software "PropCalc". A 330 mm duct fan system was developed to validate the design scheme, and static performance testing was performed on a test bench. The comparison of the experimental and theoretical results demonstrates that the theoretical method accurately predicts the DFLS' power-thrust performance with an average difference of less than 1.9%. Additionally, this paper refers to the numerical calculation method when evaluating the ducted fan scheme. Compared to the theoretical result, CFD analysis provides less accuracy in designing the DFLS, even when time and evaluation costs are ignored.

Finally, the rotational speed characteristics of the ducted fan are discussed in hover, and the concept of directly referring to the unducted result at the same power is advanced. In general, the aerodynamic design and evaluation method for the DFLS proposed in this paper is simple, quick, and practical. Although this method has been validated only in the context of this flying car project, it is clear that it can also be used to increase the efficiency of other UAM development. This research has raised numerous unanswered questions. Additional work will be required to establish and quantify use boundaries, as well as to develop and test a full-size DFLS.

## Declaration of conflicting interests

The author(s) declared no potential conflicts of interest with respect to the research, authorship, and/or publication of this article.

## Funding

The author(s) disclosed receipt of the following financial support for the research, authorship, and/or publication of this article: This work is sponsored by Universiti Sains Malaysia (USM) with the Short Term Research Grant Scheme [grant number: 304/PAERO/6315297] and Malaysian Ministry of Higher Education with the Fundamental Research Grant Scheme [grant number: FRGS/1/2020/TK0/USM/03/11].

## ORCID iDs

Hanjie Jiang  <https://orcid.org/0000-0001-5514-7542>

Ye Zhou  <https://orcid.org/0000-0003-3644-1847>

## References

1. Yoeli R. Ducted fan utility vehicles and other flying cars. In: 2002 Biennial International Powered Lift Conference & Exhibit, Williamsburg, Virginia, 5 November 2002–7 November 2002, pp. 1–6.
2. Straubinger A, Rothfeld R, Shamiyeh M, et al. An overview of current research and developments in urban air mobility—Setting the scene for UAM introduction. *J Air Transport Manage* 2020; 87(101852): 1–12.
3. Zhou Y, Zhao H and Liu Y. An evaluative review of the VTOL technologies for unmanned and manned aerial vehicles. *Comput Commun* 2020; 149: 356–369.

4. Jiang Y, Zhang B and Huang T. CFD study of an annular-ducted fan lift system for VTOL aircraft. *Aerospace* 2015; 2: 555–580.
5. Ahn J and Lee K. Performance prediction and design of a ducted fan system. In: AIAA/ASME/SAE/ASEE Joint Propulsion Conference & Exhibit, Fort Lauderdale, Florida, 11 July 2004–14 July 2004, pp. 1–9.
6. Taylor RT. *Experimental investigation of the effects of some shroud design variables on the static thrust characteristics of a small-scale shrouded propeller submerged in a wing*, Technical Report Archive & Image Library, 1958, Vol. 8, pp. 41–50.
7. Fan N-J, Xu J and Yang J-W. Numerical study on aerodynamic characteristics of ducted fan aircraft. *J Beijing Institute Technol* 2010; 19: 19–24.
8. Pflimlin J-M, Binetti P, Souères P, et al. Modeling and attitude control analysis of a ducted-fan micro aerial vehicle. *Control Eng Pract* 2010; 18: 209–218.
9. Eriksson M and Wedell B. *Performance Estimation of a Ducted Fan UAV*. Linköping University, Department of Electrical Engineering, 2006.
10. Ruzicka G, Meadowcroft E and Strawn R. Discrete-blade, navier-stokes computational fluid dynamics analysis of ducted-fan flow. *J Aircraft* 2005; 42: 1109–1117.
11. Bo W, Zheng G, Peng W, et al. Investigation of the aerodynamic characters of ducted fan system. *Int J Aerospace Mech Eng* 2012; 6(9): 2015–2018.
12. Schenk H. *The Introduction of PropCalc*, 2007, pp. 1–6.
13. Grahame W. Aerodynamic effects of lift-jet and lift-fan inlets in transition flight. *J Aircraft* 1969; 6: 150–155.
14. Platt RJJ. Static tests of a shrouded and an unshrouded propeller. Technical Report Archive & Image Library, No. L7H25, 1948, pp. 1–40.
15. Sheng C and Zhao Q. Numerical investigations of fan-in-wing aerodynamic performance with active flow control. In 34th AIAA Applied Aerodynamics Conference, Washington, DC, 13–17 June 2016, pp. 1–14.
16. Xu He-yong YZy. Numerical simulation and comparison of aerodynamic characteristics of ducted and isolated propellers. *J Aerospace Power* 2011; 26(12): 6.
17. Fenwick C and Allen C. Development and validation of sliding grid technology for time-domain aeroservoelastic simulations. In: 23rd AIAA Applied Aerodynamics Conference, Toronto, Canada, 6 June 2005–9 June 2005. American Institute of Aeronautics and Astronautics Inc. AIAA, United States, 2005, pp. 1–16 [Conference Organiser: AIAA Other identifier: (AIAA) 2005-4844].